VO_2 thermo-chromic metamaterial-based smart optical solar reflector

Kai Sun, [1,2] Christoph A. Riedel,[1,2] Alessandro Urbani,[3] Mirko Simeoni,[3] Sandro Mengali,[3] Maksim Zalkovskij,[4] Brian Bilenberg,[4] C.H. de Groot,[,1] and Otto L. Muskens*[,2]*

[1] Electronics and Computer Science, Faculty of Physical Sciences and Engineering, University of Southampton, Southampton SO17 1BJ, United Kindom

[2] Physics and Astronomy, Faculty of Physical Sciences and Engineering, University of Southampton, Southampton, SO17 1BJ, United Kindom

[3] Consorzio CREO, SS.17 Località Boschetto, 1-67100, L'Aquila, Italy

[4] NIL Technology, Diplomvej 381, 2800 Kongens Lyngby, Demark

ABSTRACT: Optical solar reflector smart radiators are able to control the temperature of spacecraft. This work demonstrates a novel smart optical solar reflector using a patterned thermo-chromic VO_2 plasmonic meta-surface design. The VO_2 meta-surface combines the temperature induced phase transition of VO_2 with plasmonic resonances resulting in a significant enhancement of the infrared absorption. The enhanced absorption obtained at a reduced VO_2 coverage results in superior emittance tunability $\Delta\varepsilon$ and lower solar absorptance α compared to a corresponding thin-film reflector. An emittance tunability of 0.48 is obtained for the meta-reflector design, representing a 30% improvement compared to the unstructured film. Meta-surface based smart optical solar reflectors offer a new route toward energy-efficient and cost-effective passive thermal control systems of spacecraft and other surfaces.

KEYWORDS: Keywords: plasmonics, optical solar reflectors, thermochromic materials, radiative cooling, meta-surfaces, metamaterial perfect absorber

Spacecraft and satellites require internal temperature control to minimize thermal fluctuations, which relaxes the thermal-mechanical constraints and increase the lifetime of the electronic devices. An optical solar reflector (OSR) is a spectrally selective filter, that reflects the optical spectrum corresponding to the radiation spectrum of the sun (solar absorptance α), and emits the thermal infrared spectrum corresponding to that of a black body at 300K (emittance ε) Radiative cooling through high-emissivity surfaces consitutes an effective approach of dissipating energy produced by on-board instruments and electronics while minimizing solar absorption. The drawback of such high-emissivity surfaces is that they dissipate precious heat during the initial start-up phase, eclipses, or when the instrumentation is in sleep or safe mode.[1] Stabilization of the spacecraft temperature against such varying conditions requires a thermal control system to maintain the temperature in an optimal range. An active system normally involves temperature sensors, control circuits and moving parts[2, 3] which add to overall cost of the mission while reducing the payload capacity. Passive or smart systems are based on materials which show a temperature dependent emittance.[4, 5] Compared with the active thermal control system, the passive control system is advantageous for its simplicity, reduced weight and lower costs. A smart control system requires the emittance at low temperatures ε_{cold} to be low to keep the heat, and the emittance at high temperatures ε_{hot} to be high to dissipate surplus heat. The smart control system performance is normally described by its dynamic tunability of emittance $\Delta\varepsilon = \varepsilon_{hot} - \varepsilon_{cold}$.[1, 6, 7]

Vanadium dioxide (VO_2) is an ideal material for the smart thermal control system due to its thermochromic characteristics. VO_2 has a semiconductor-to-metal phase transition at a critical temperature of around 68°C.[8-10] By doping VO_2 with elements such as tungsten, or by using defect engineering, the transition temperature can be reduced towards room temperature.[9, 11] As a thermochromic material compatible with the harsh requirements of the space environment,[11] VO_2 has been intensively investigated as a reflector for passive thermal control. Reflectors with VO_2 deposited directly on an aluminum substrate have been reported to give a tunability $\Delta\varepsilon$ of 0.21 to 0.34.[1, 12] With an insulator between VO_2 and the aluminum reflector, a destructive interference pattern can be formed to further improve the absorption around the peak of the blackbody spectrum.[6, 7, 9] While good tunability was demonstrated using low-emissivity dielectrics, the high-temperature emittance of such a thin film planar design is limited to around ε_{hot} = 0.6 - 0.7 by the spectral bandwidth of the thin-film interference mechanism. Higher performance may be obtained by using a broadband

multilayer stack,[13] at the cost of increased thickness and added complexity of use, e.g., in flexible foils.

Several studies have reported the effects of a global, thermally or optically driven phase transition in VO_2 on the plasmonic response of nanoparticles and metamaterials over a broad spectral range from terahertz,[14-17] mid-infrared,[18, 19] near-infrared[20-23] to visible.[23-25] In the visible and near-infrared, studies of plasmonic effects on the optical excitation of the IMT have focused on hot-electron injection-driven ultrafast processes[26, 27] and on non-resonant, continuous-wavemediated plasmonic heating,[21, 28] including our demonstration of picosecond control of switching.[29]

In this work, we demonstrate a unique practical application in the form of a thin smart optical solar reflector based on a VO_2 meta-surface (meta-OSR) which combines the benefits from thermo-chromic and plasmonic properties. The improved performance in our devices is based on plasmonic resonance effects[30] which cause an increased absorption of the structured surface in the high-temperature metallic state of VO_2, while the low-temperature emittance and solar absorptance is reduced due to a partial VO_2 coverage. Compared to the corresponding smart thin-film design, the smart meta-OSR achieves a superior tunability range $\Delta\varepsilon$ at reduced solar absorptance.

Results and Discussion

The smart meta-OSR design, shown schematically in **Figure 1**a, consists of a back-reflector, a SiO_2 spacer, and a VO_2 meta-surface. The 1200 nm SiO_2 spacer thickness provides a maximum absorption effect in the range of the thermal blackbody spectrum when VO_2 is in the metallic phase ('hot' state). The VO_2 meta-surface consists of an array of squares with size *L* varying from 1.6 to 2.8 μm. **Figure 1b** shows calculated emittance for a square size of 2.6 μm with a gap between adjacent squares of 1.0 μm. The low-temperature response is characterized by a peak at around 10 μm wavelength, corresponding to the infrared TO phonon band of the SiO_2 spacer, and a low emittance in other parts of the spectrum. In the high-temperature state, the overall emittance is high over a wide spectral range from 5 - 20 μm, the region corresponding to the thermal blackbody emission. In comparison, a continuous

thin-film structure of the same layer thickness (dashed lines) shows much lower emittance values over this range. Maps of the electric field normal to thethe surface of the VO_2 element are shown in Figure 1c for both the hot state and the cold state . The high-temperature field profiles are indicative of a half-wavelength ($\lambda/2$) dipolar resonance with a full width spanning from 5-15 μm, i.e. on both sides of the SiO_2 phonon line. This large resonance bandwidth results from a combination of the specific resonator design, ohmic losses in the metallic VO_2, and the particular dispersion of the SiO2 permittivity.[30] At low temperatures, the VO_2 is dielectric and much lower local fields are obtained which do not show an effect of resonance contribution. In Figure 1d we plot the local absorption coefficient Q_{abs}, which is defined as the dissipated power density normalized to an incident flux of 1 W/m^2. A large increase of the absorbed power in the high-temperature metallic state of the VO_2 confirms the resonant absorption characteristics of the design.

Smart meta-OSRs were fabricated on top of a silicon substrate using e-beam lithography as described in the Experimental Section. Thermochromic films of VO_2 of 50 nm thickness were obtained by deposition of a 20 nm metallic vanadium film, followed by a thermal oxidation process.[31-33] Good performance of the VO_2 layers was verified using the thermochromic response, as well as using Raman spectroscopy (see Supporting Information Figure S6).
SEM images of the experimental structures are presented in **Figure 2.** The cross section of the smart meta-OSR is given in Figure 2a and shows the subsequent layers in the stack. Good mechanical adhesion between the different layers is obtained, which is an important parameter for producing a mechanically robust technology. The top-view SEM images in Figure 2b show good quality of the e-beam and etching process resulting in well-defined geometries over the range of feature sizes *L* from 1.6 μm to 2.8 μm and gap widths *d* from 0.5 μm to 2.0 μm. .

Figure 3 shows both the VIS/NIR and the FTIR absorption spectra of the fabricated VO_2 reflectors measured at temperatures of 80°C (Figure 3a,c) and 25°C (Figure 3b,d) and for various lengths *L* at fixed gap *d* = 0.5 μm (Figure 3a,b) and for various *d* at fixed *L* of 2.8 μm (Figure 3c,d). The low temperature spectra show low absorption in the infrared except for the strong bands at 8 μm, 10 μm, and 12.5 μm, which can be attributed to infrared absorption of the SiO_2 spacer.[34] The patterned VO_2 shows lower absorption than the planar film which is related to the reduction in VO_2 coverage. At high temperature, all spectra show a strong increase in absorption over a broad range of wavelength. The spectra for the planar VO_2 film

are consistent with published work on similar structures.[35] The meta-OSR structures show an increased absorption in the wavelength ranges 4-7 μm and 12-15 μm, while a reduced performance is observed around the dip centered at 18 μm. The latter feature can be attributed to oxygen vibrational resonances in the VO_2 lattice.[36] The additional absorption at 4-15 μm around the peak of the black-body spectrum, is related to the plasmonic λ/2 resonance mode in the square array as was discussed in **Figure 1b**. This mode becomes broader, more intense and shifts to longer wavelengths for the larger squares. As shown in **Figure 3c**, decreasing the gap size *d* has a similar effect as increasing length L with the plasmonic resonance intensifying, broadening, and shifting to longer wavelength. These changes of the absorption spectrum with gap width and feature size involve a combination of effects that include dipolar coupling between elements in the array, shifts in the perfect absorption condition, and changes in VO_2 coverage.

From the FTIR reflectivity spectra, the emissivity values can be extracted using equation 1 and these are shown in **Figure 4a**. At low temperature, the emissivity ε_{cold} of the patterned films is considerably lower than that for the planar film. This is advantageous as it will reduce radiative cooling at low temperatures. For the patterned films, increasing feature size from 1.6 to 2.8 μm results in a slightly increased ε_{cold} for all gaps due to increased VO_2 coverage.

At high temperature, emissivity ε_{hot} of the planar films is higher than for most patterned films due to the reduced absorption above 18 μm wavelength in the patterned films. However, for the structures with smallest gap of d = 0.5 μm and with feature sizes L of 2.4 and 2.8 μm, emissivity at high temperature is substantially higher for the patterned film than the planar film. In fact, the emittance tunability $\Delta\varepsilon$, shown in **Figure 4b**, shows that the tunability of the patterned films outperforms the planar films over a much wider pattern range. The $\Delta\varepsilon$ curves unambiguously show that all square arrays with 0.5 μm gap have an enhanced emittance tunability compared to the planar structure with the largest $\Delta\varepsilon$ of 0.48 for the largest feature size of 2.8 μm. This is a 30% improvement over the planar film structure with $\Delta\varepsilon$ of 0.37. For larger gap dimensions, a similar trend is seen, but at a lower overall tunability. Our reported $\Delta\varepsilon$ of 0.48 equals the best literature value of unpatterned films obtained using a low-emissivity HfO_2 dielectric spacer.[7] We expect that further improvements will be achievable when combining our meta-OSR concepts with such specialized low-emittance materials.

Figure 4c shows the extracted solar absorptance α as a function of feature size for VO_2 reflectors at different gaps measured at 25°C and 80°C. For all arrays, absorptance is considerably higher at 80°C than at 25°C. The increase of absorptance at high temperature is consistent with the increase of the imaginary part of the permittivity (see Supplementary Information). At both temperatures, absorptance of the square arrays is seen to decrease with the increase of gap size from 0.5 to 2 μm. Compared with the planar film structure, arrays with 1 and 2 μm gap give lower absorptance whilst the 0.5 μm gaps gives a similar absorptance. The decrease in absorptance is related to the VO_2 coverage.

We note that other studies on VO_2 radiative cooling devices have not reported values for solar absorptance, therefore it is not possible to directly compare values reported in this work to other designs. However, it is expected that the UV-visible absorptance is proportional to VO_2 coverage and thickness. This scaling is illustrated in **Figure 4d** which shows the absorptance α and the emittance tunability Δε plotted against the VO_2 area coverage of the arrays. Indeed, the solar absorptance follows a monotonous trend with area coverage, where the highest absorption is obtained for the continuous film and α is reduced by patterning. In contrast, the trends observed in the emissivity contrast do not follow such a simple scaling but follow the electromagnetic resonances of the meta-surface, significantly exceeding the thin film result.

To demonstrate the scale-up capability, the smart meta-OSR array was fabricated onto a 20 × 20 mm substrate using large-area e-beam lithography. Figure 5a shows the SEM micrograph of the patterned VO_2 smart meta-OSRs, where the square array is well defined in dimension of about 2.7 μm with a gap of 0.5 μm with the meta-OSR substrate photo shown in the inset of Figure 5a. The infrared absoprtion was measured using FTIR over a temperature cycle up and down from 25°C to 90°C. Figure 5b shows the absorption spectra of the smart OSR at 25°C, 40°C, 60°C, 70°C and 80°C,with the calculated emissivity shown in Figure 5c. We find excellent performance of the large-area device in line with the small-area test structures. The phase transition shows its characteristic first order hysteresis, with a transition temperature in the range of 65°C -70°C and a temperature width of the hysteresis region of 23°C, which is consistent with good quality VO_2.[8, 9] The curve of Δε clearly demonstrates the emissivity response of the smart-OSR to the temperature change and Δε is calculated to be 0.43 from 25°C to 90°C.

Further improvement of the performance of VO_2 smart meta-OSRs will involve the use of low-emissivity materials for the dielectric spacer, and the addition of interference filters to reduce α. Ultimately, large-area devices can be fabricated using scaled-up techniques such as nano-imprint lithography. Given the high costs associated with assembly and launch of spacecraft, it is anticipated that such a nanotechnology approach can be cost effective. Other applications in radiative cooling can be envisaged, for example in airplanes or even terrestrial applications, but will require additional design and optimization to account for atmospheric contributions in the thermal emissivity, which goes beyond the current study.

In conclusion, smart meta-reflectors based on VO_2 have been proposed and successfully fabricated with patterns of various dimensions. The infrared response shows all meta-reflectors give lower emittance than the planar film reflector at low temperature whilst meta-reflectors with high VO_2 coverage give higher emittance than the planar film reflector at high temperature. Particularly, those meta-reflectors can improve the performance of emittance tunability $\Delta\varepsilon$ to 0.48 compared to 0.37 for the planar reflector. The emittance improvement for a meta-reflector at high temperature is attributed to the plasmonic resonances in the patterned VO_2, which is set around the peak of the black-body spectrum. UV/VIS absorptance is lower for the meta-reflector structures than for planar films further enhancing the positive effect of the meta-reflectors for smart optical solar reflectors. Our plasmonic approach to enhance functionality can be applied to all similar solar reflectors with smart materials.

Methods

Fabrication of smart meta-OSR. The meta-OSR structures were fabricated on a silicon substrate, which was coated with a 50 nm thin Al_2O_3 film deposited using reactive sputtering. The structure consists of an sputtered aluminium film of 80 nm thickness as an optical back-reflector, followed by a 1200 nm SiO_2 spacer obtained using plasma-enhanced chemical vapor deposition (PECVD) at 350°C. A 20 nm vanadium film was sputtered onto the SiO_2 spacer at room temperature and was subsequently converted into 50 nm VO_2 under O_2 ambient at 375°C. A 6 nm Al_2O_3 capping layer was deposited by a thermal atomic layer deposition (ALD) process at 200 °C using a Savannah ALD system. The capping layer was used for better adhesion to the e-beam resist. The thermochromic phase transition of the thin film as measured by emittance and resistivity is displayed in Supporting Information Figure S3. The Al_2O_3/VO_2 layers were subsequently patterned by e-beam lithography using a JEOL JBX-

9300 electron beam system, e-beam resist ZEP520A, and ion beam etching (IBE). The IBE was carried out in an OIPT IonFab 300 plus system using a highly transferable Argon physical etching process.[30] The etching rates were measured to be 4.3 nm/min and 6.4 nm/min for Al_2O_3 and VO_2, respectively. The resist ZEP was subsequently stripped by an ultra-sonic bath in NMP at 50°C for about 4 hours. The VO_2 meta-surface was designed and fabricated as an array of squares with lengths *L* varying from 1.6 to 2.8 μm in steps of 0.4 μm. For each square size, three different values of the gap *d* between the squares were chosen of respectively 0.5, 1 and 2 μm. All experimental dimensions were within 5% of the designed length and gap values. Each meta-OSR array covers 120 × 120 μm^2, sufficient for both UV-Visible and infrared optical characterizations as shown in Supporting Information Figure S5.

Infrared characterization and determination of ε. To obtain the emittance *ε*, the IR reflectance was measured in the range of 2.5 to 25 μm using an FTIR setup consisting of a Thermo-Nicolet Nexus 670 with a Continuum microscope, far-IR light source, KBr beam splitter and nitrogen-cooled DTGS detector with a spot size of 100×100 μm^2. For all measurements, an 80 nm aluminium coated SiO_2/Si substrate was used as reference mirror. According to Kirchhoff's law, the spectral emittance and spectral absorptance of a body are equal at thermal equilibrium condition. For a IR opaque reflector without transmission, the emissivity, *ε(λ)*, can be described using the relation: $\varepsilon(\lambda) = 1 - R(\lambda)$, where *R(λ)* is the reflectivity. The emittance is defined as the averaging emissivity weighted by the theoretical blackbody spectrum at the operating temperature (T) in Kelvin:[37]

$$\varepsilon = \frac{\int (1 - R(\lambda)) B(\lambda, T) d\lambda}{\int B(\lambda, T) d\lambda}, \quad (1)$$

where *B*(λ, T) is the blackbody spectral distribution at temperature *T*, given by Plank's equation. In this work, the integration range is the set FTIR measurement range from 2.5 to 25 μm in accordance with European space Agency (ESA) standards[38] and *T* is set as 25°C (referred as low temperature) and 80°C (referred as high temperature) corresponding to the semiconductor phase and metallic phase of VO_2, respectively. The chosen range includes 83% of the total black body energy with less than 0.1% not included on the short-wavelength side and 17% on the long wavelength side. The shift in black body spectrum between both temperatures is minor and contributes only 2% to the tunability Δε.

Optical characterization and determination of α. To get the solar absorptance α of the small-area devices, the VIS/NIR reflectance was measured using a home-built total reflection setup based on a 4-inch integrating sphere (Bentham, Supporting Information Figure S3), which is designed to trap high angle scattering. The measurements of α were done using a combination of a broadband supercontinuum light source and prism spectrometer spanning a wavelength range of 0.48 to 1.8 μm, employing a Si detector for 0.48-0.9 μm and an InGaAs detector for 0.9-1.8 μm. For all measurements, a white $BaSO_4$ reference surface was used. Like emissivity, the solar absorptance is the averaging emissivity weighted by the solar irradiance distribution using Equation 1, where $B(\lambda)$ is now the spectral solar irradiance at 5777 K. In this work, the integration range is the set UV/NIR measurement range from 0.48 to 1.8 μm as a shortened range.[38] This includes 70% of the total energy of the solar spectra, with 22% being left at the short-wavelength side and 8% at the long wavelength.

Numerical modelling. For numerical simulations of meta-OSRs we used both finite element (COMSOL 5.3) and finite-difference time domain (FDTD, Lumerical) modelling. Lumerical FDTD was used to simulate broadband spectra from 0.2-30 μm. For the detailed near-field maps, we used COMSOL finite element modelling, which was confirmed to give identical results to the FDTD in the infrared spectral range. In both cases we used linearly polarized incident light. VO_2 antennas were modelled as squares with rounded top edges using a radius of curvature of 20 nm. We used tabulated values of the dielectric function of VO_2 in the cold and hot-states.[39]

Supporting Information

All data supporting this study are openly available from the University of Southampton repository at https://doi.org/10.5258/SOTON/D0226.

Author Information

Corresponding Authors

*E-mail: chdg@ecs.soton.ac.uk (CHG)

* E-mail: o.muskens@soton.ac.uk (OM)

Author Contributions

K.S., S.M., C.H.G. and O.M. conceived the experiment. A.U. and M.S. performed the VO_2 stack layer fabrication using sputtering. K.S. performed the e-beam lithography and rest fabrication processes. C.A.R. performed the Ellipsometry measurements and analyzed the Ellipsometry data. K.S. and O.M. performed the optical characterizations and data analysis. K.S., C.H.G. and O.M. wrote the manuscript with contributions from all co-authors.

Acknowledgements

This project has received funding from the European Union's Horizon 2020 research and innovation programme under Grant Agreement N° 687303 "METAREFLECTOR" and EPSRC and EP/J016918/1.

References

1. Haddad, E.; Kruzelecky, R.; Wong, B.; Jamroz, W.; Soltani, M.; Chaker, M.; Benkahoul, M.; Poinas, P., Tuneable emittance thin film coatings for thermal control. In *7th ISMSE*, Aix-en-Provence, France, 2009.
2. Osiander, R.; Firebaugh, S. L.; Champion, J. L.; Farrar, D.; Darrin, M. A. G. Microelectromechanical devices for satellite thermal control. *IEEE Sens. J.* **2004,** 4, (4), 525-531.
3. Demiryont, H.; Shannon, K.; Ponnappan, R. Electrochromic Devices for Satellite Thermal Control. *Space Technology and Applications International Forum - Staif 2006* **2006,** 813, 64-73.
4. Shimakawa, Y.; Yoshitake, T.; Kubo, Y.; Machida, T.; Shinagawa, K.; Okamoto, A.; Nakamura, Y.; Ochi, A.; Tachikawa, S.; Ohnishi, A. A variable-emittance radiator based on a metal-insulator transition of (La,Sr)MnO3 thin films. *Appl Phys Lett* **2002,** 80(25), 4864-4866.
5. Leahu, G. L.; Li Voti, R.; Larciprete, M. C.; Belardini, A.; Mura, F.; Fratoddi, I.; Sibilia, C.; Bertolotti, M. Semiconductor-metal phase transition of vanadium dioxide nanostructures on silicon substrate: Applications for thermal control of spacecraft. *Aip Conf Proc* **2014,** 1603, 62-70.
6. Haddad, E.; Kruzelecky, R. V.; Hendaoui, A.; Chaker, M.; Jamroz, W.; Poinas, P., Large Tuneability IR Emittance Thermal Control Coating for Space Applications. In *43rd International Conference on Environmental Systems*, American Institute of Aeronautics and Astronautics: 2013.
7. Wang, X.; Cao, Y. Z.; Zhang, Y. Z.; Yan, L.; Li, Y. Fabrication of VO2-based multilayer structure with variable emittance. *Appl Surf Sci* **2015,** 344, 230-235.
8. Chain, E. E. Optical properties of vanadium dioxide and vanadium pentoxide thin films. *Appl Optics* **1991,** 30 (19), 2782-2787.
9. Hendaoui, A.; Emond, N.; Dorval, S.; Chaker, M.; Haddad, E. VO2-based smart coatings with improved emittance-switching properties for an energy-efficient near room-temperature thermal control of spacecrafts. *Sol. Energ. Mat. Sol. Cell* **2013,** 117, 494-498.
10. Morin, F. J. Oxides Which Show a Metal-to-Insulator Transition at the Neel Temperature. *Phys Rev Lett* **1959,** 3 (1), 34-36.
11. Rensberg, J.; Zhang, S.; Zhou, Y.; McLeod, A. S.; Schwarz, C.; Goldflam, M.; Liu, M. K.; Kerbusch, J.; Nawrodt, R.; Ramanathan, S.; Basov, D. N.; Capasso, F.; Ronning, C.; Kats, M. A. Active Optical Metasurfaces Based on Defect-Engineered Phase-Transition Materials *Nano Lett.* **2016,** 16 (2), 1050-1055.

12. Benkahoul, M.; Chaker, M.; Margot, J.; Haddad, E.; Kruzelecky, R.; Wong, B.; Jamroz, W.; Poinas, P. Thermochromic VO 2 film deposited on Al with tunable thermal emissivity for space applications. *Sol Energ Mat Sol C* **2011,** 95, (12), 3504-3508.
13. Keller, J. G.; Moy, R. M.; Felland, J. R. Thermal control coatings. US Patent 7691435, 2010.
14. Driscoll, T.; Kim, H. T.; Chae, B. G.; Kim, B. J.; Lee, Y. W.; Jokerst, N. M.; Palit, S.; Smith, D. R.; Di Ventra, M.; Basov, D. N. Memory metamaterials. *Science* **2009,** 325, (5947), 1518-1521.
15. Liu, M.; Hwang, H. Y.; Tao, H.; Strikwerda, A. C.; Fan, K.; Keiser, G. R.; Sternbach, A. J.; West, K. G.; Kittiwatanakul, S.; Lu, J.; Wolf, S. A.; Omenetto, F. G.; Zhang, X.; Nelson, K. A.; Averitt, R. D. Terahertz-field-induced insulator-to-metal transition in vanadium dioxide metamaterial. *Nature* **2012,** 487, (7407), 345-348.
16. Seo, M.; Kyoung, J.; Park, H.; Koo, S.; Kim, H. S.; Bernien, H.; Kim, B. J.; Choe, J. H.; Ahn, Y. H.; Kim, H. T.; Park, N.; Park, Q. H.; Ahn, K.; Kim, D. S. Active terahertz nanoantennas based on VO2 phase transition. *Nano Lett* **2010,** 10, (6), 2064-2068.
17. Thompson, Z. J.; Stickel, A.; Jeong, Y. G.; Han, S.; Son, B. H.; Paul, M. J.; Lee, B.; Mousavian, A.; Seo, G.; Kim, H. T.; Lee, Y. S.; Kim, D. S. Terahertz-Triggered Phase Transition and Hysteresis Narrowing in a Nanoantenna Patterned Vanadium Dioxide Film. *Nano Lett* **2015,** 15, (9), 5893-5898.
18. Kats, M. A.; Blanchard, R.; Genevet, P.; Yang, Z.; Qazilbash, M. M.; Basov, D. N.; Ramanathan, S.; Capasso, F. Thermal tuning of mid-infrared plasmonic antenna arrays using a phase change material. *Opt Lett* **2013,** 38, (3), 368-370.
19. Shelton, D. J.; Coffey, K. R.; Boreman, G. D. Experimental demonstration of tunable phase in a thermochromic infrared-reflectarray metamaterial. *Opt Express* **2010,** 18, (2), 1330-1335.
20. Dicken, M. J.; Aydin, K.; Pryce, I. M.; Sweatlock, L. A.; Boyd, E. M.; Walavalkar, S.; Ma, J.; Atwater, H. A. Frequency tunable near-infrared metamaterials based on VO2 phase transition. *Opt Express* **2009,** 17, (20), 18330-18339.
21. Lei, D. Y.; Appavoo, K.; Ligmajer, F.; Sonnefraud, Y.; Haglund, R. F.; Maier, S. A. Optically-Triggered Nanoscale Memory Effect in a Hybrid Plasmonic-Phase Changing Nanostructure. *ACS Photonics* **2015,** 2, (9), 1306-1313.
22. Son, T. V.; Ba, C. O. F.; Vallee, R.; Hache, A. Nanometer-thick flat lens with adjustable focus. *Appl Phys Lett* **2014,** 105, 231120.
23. Guo, P. J.; Weimer, M. S.; Emery, J. D.; Diroll, B. T.; Chen, X. Q.; Hock, A. S.; Chang, R. P. H.; Martinson, A. B. F.; Schaller, R. D. Conformal Coating of a Phase Change Material on Ordered Plasmonic Nanorod Arrays for Broadband All-Optical Switching. *ACS Nano* **2017,** 11, (1), 693-701.
24. Lei, D. Y.; Appavoo, K.; Sonnefraud, Y.; Haglund, R. F.; Maier, S. A. Single-particle plasmon resonance spectroscopy of phase transition in vanadium dioxide. *Opt Lett* **2010,** 35, (23), 3988-3990.
25. Appavoo, K.; Haglund, R. F. Polarization selective phase-change nanomodulator. *Sci Rep.* **2014,** 4, 6771.
26. Appavoo, K.; Wang, B.; Brady, N. F.; Seo, M.; Nag, J.; Prasankumar, R. P.; Hilton, D. J.; Pantelides, S. T.; Haglund, R. F. Ultrafast phase transition via catastrophic phonon collapse driven by plasmonic hot-electron injection. *Nano Lett* **2014,** 14, (3), 1127-1133.
27. Hada, M.; Zhang, D. F.; Casandruc, A.; Miller, R. J. D.; Hontani, Y.; Matsuo, J.; Marvel, R. E.; Haglund, R. F. Hot electron injection driven phase transitions. *Phys Rev B* **2012,** 86, (13).
28. Ferrara, D. W.; MacQuarrie, E. R.; Nag, J.; Kaye, A. B.; Haglund, R. F. Plasmon-enhanced low-intensity laser switching of gold::vanadium dioxide nanocomposites. *Appl Phys Lett* **2011,** 98, (24).

29. Muskens, O. L.; Bergamini, L.; Wang, Y. D.; Gaskell, J. M.; Zabala, N.; de Groot, C. H.; Sheel, D. W.; Aizpurua, J. Antenna-assisted picosecond control of nanoscale phase transition in vanadium dioxide. *Light-Sci Appl* **2016,** 5.
30. Sun, K.; Riedel, C. A.; Wang, Y.; Urbani, A.; Simeoni, M.; Mengali, S.; Zalkovskij, M.; Bilenberg, B.; de Groot, C. H.; Muskens, O. L. Metasurface optical solar reflectors using AZO transparent conducting oxides for radiative cooling of spacecraft. *ACS Photonics* **2018**, 5, 495-501
31. Gurvitch, M.; Luryi, S.; Polyakov, A.; Shabalov, A.; Dudley, M.; Wang, G.; Ge, S.; Yakovlev, V. VO2 films with strong semiconductor to metal phase transition prepared by the precursor oxidation process, *J. Appl. Phys.* **2007**, 102, 033504.
32. Lee, S; Meyer, T. L.; Park, S.; Egami, T.; Lee, H. N. Growth control of the oxidation state in vanadium oxide thin films, *Appl. Phys. Lett.* **2014**, 105, 223515.
33. Liu, X; Wang, S.-W.; Chen, F.; Yu, L.; Chen, X. Tuning phase transition temperature of VO2 thin films by annealing atmosphere, *J. Phys. D: Appl. Phys.* **2015**, 48, 265104.34.
Gunde, M. K. Vibrational modes in amorphous silicon dioxide. *Physica B* **2000,** 292, (3-4), 286-295.
35. Hendaoui, A.; Emond, N.; Chaker, M.; Haddad, E. Highly tunable-emittance radiator based on semiconductor-metal transition of VO2 thin films. *Appl Phys Lett* **2013,** 102, (6), 061107.
36. Gervais, F.; Kress, W. Lattice dynamics of oxides with rutile structure and instabilities at the metal-semiconductor phase transitions of NbO2 and VO2. *Phys Rev B* **1985,** 31 (8), 4809-4814.
37. Breuch, R. A.; Marshall, K. N. Studies on the effects of the interplanetary space environment on thermal-control coatings. *J. Spacecraft and Rockets* **1968,** 5, (9), 1051-1056.
38. ECSS-Q-ST-70-09C *ESA Space product assurance—Measurements of thermo-optical properties of thermal control materials*; ECSS-Q-ST-70-09C July 2008.
39. Verleur, H. W.; Barker, A. S.; Berglund, C. N. Optical Properties of VO2 between 0.25 and 5 eV, *Physical Review* **1968,** 172 (3), 788-798.

[1] Petrov, G.I.; Yakovlev, V.V.; Squier, Raman microscopy analysis of phase transformation mechanisms in vanadium dioxide, J. Appl. Phys. Lett., 81, 1023-1025 (2002)

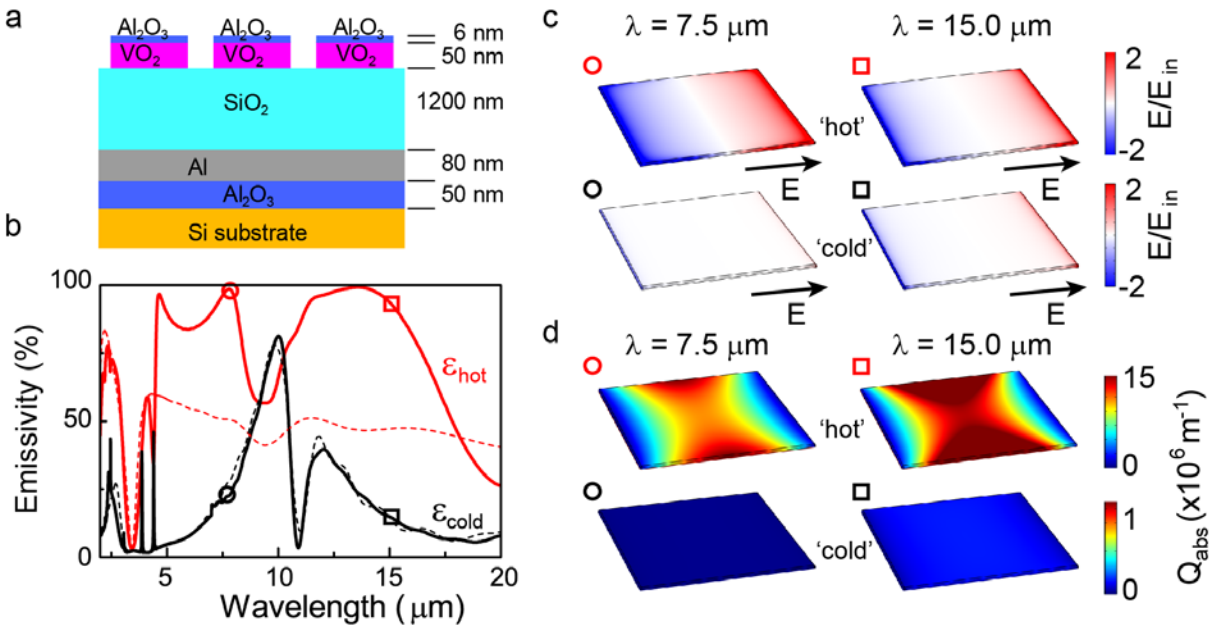

Figure 1 (a) Schematic of the VO_2 meta-material optical solar reflector or meta-reflector and (b) Calculated emissivity spectra (1-R) for meta-OSR with feature size of 2600 nm and 1000 nm gap, for temperature below the SMT (black, low-T) and above the SMT (red, high-T). Dashed lines: thin film stack without patterning of meta-surface. (c) Calculated normal near field (E/E_{in}) at VO_2 surface for wavelengths of 7.5 μm and 15 μm in 'hot' and 'cold' states, arrows correspond to orientation of the incident electric field. (d) Same as (c) for absorption coefficient (Q_{abs}) at the VO_2 surface for at VO_2 surface for wavelengths of 7.5 μm and 15 μm.

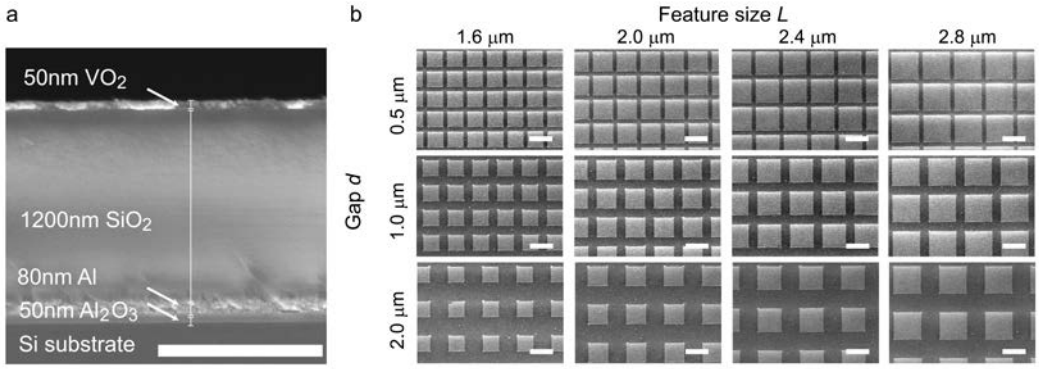

Figure 2 (a) Cross-sectional and (b) top view scanning electron microscopy (SEM) graphs of VO_2 meta-reflectors. Scale bars in (a), 1 μm and in (b), 2 μm.

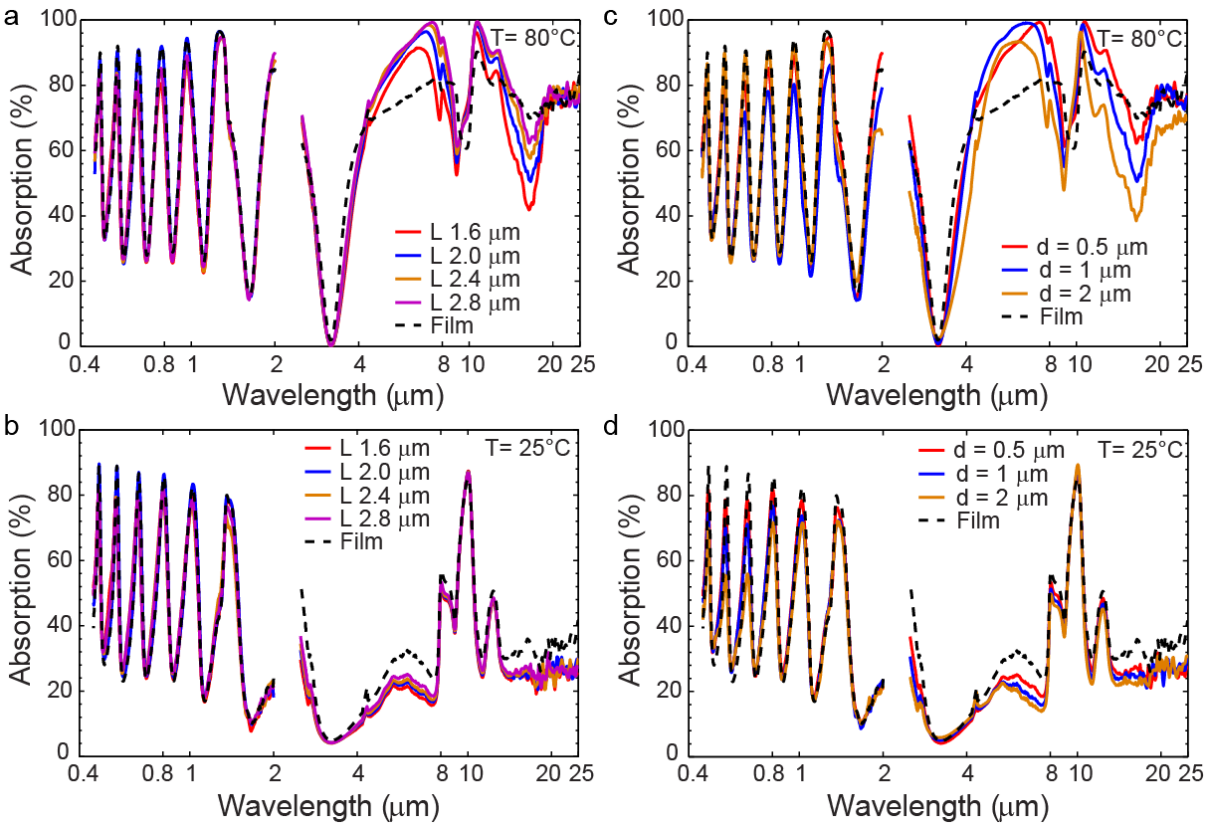

Figure 3 (a,b) Absorption spectra of VO_2 meta-reflectors with various feature sizes and a 0.5 μm gap, measured at 80°C (a) and 25°C (b). (c,d) Absorption spectra of VO_2 meta-reflectors with various gap sizes and a feature size of 2.8 μm, measured at 80°C (c) and 25°C (d). Dashed lines in (a-d) correspond to continuous film structure.

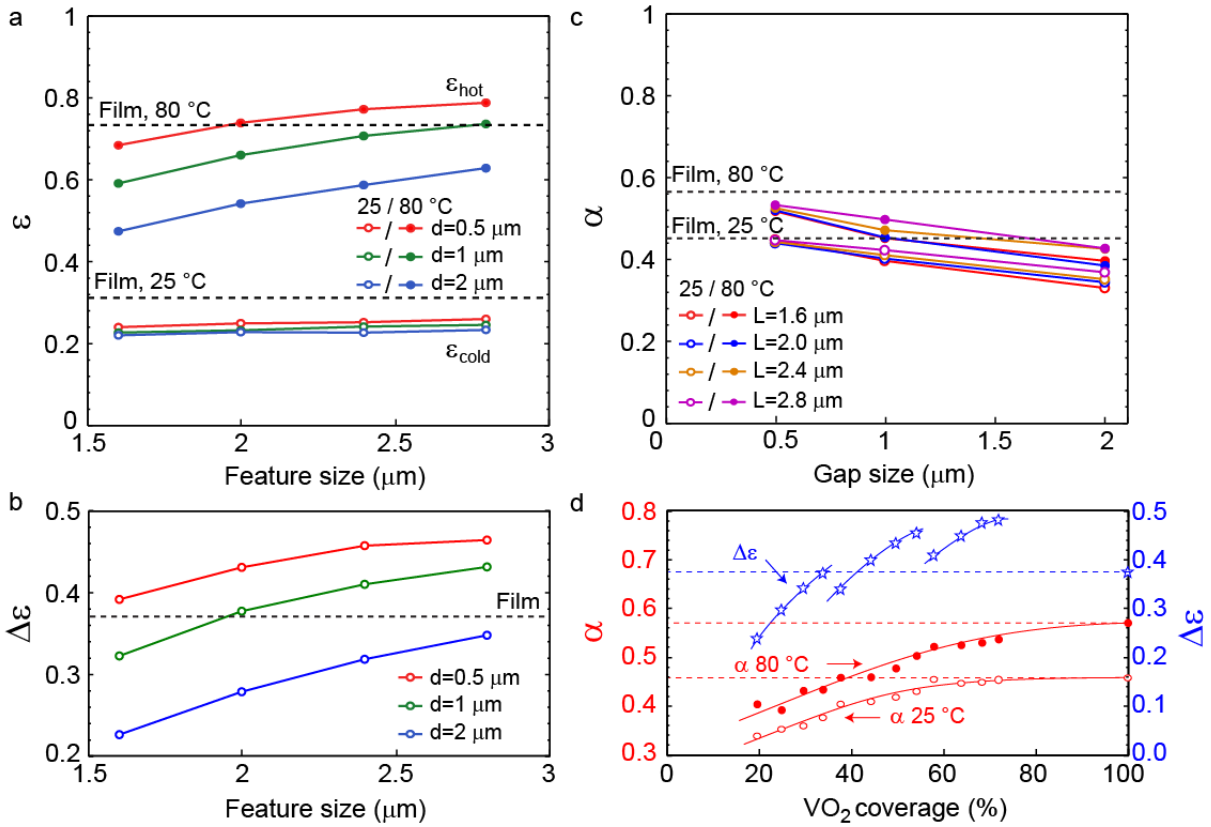

Figure 4 (a,b) Extracted emittance ε (a) and tunability Δε (b) as a function of feature size at various gap sizes of 0.5 μm, 1 μm, and 2 μm. Emittance was measured at temperatures of 25°C (ε_{cold}) and 80°C (ε_{hot}). Dashed lines, results for planar film reflector. (c) Extracted solar absorptance α as a function of gap size and for the different feature sizes, measured at temperatures of 25°C and 80°C. (d) Emittance tunability Δε and solar absorptance α plotted as a function of the VO_2 coverage. Solid lines are guides to the eye. Dashed lines are the results for planar film reflector (100% VO_2 coverage).

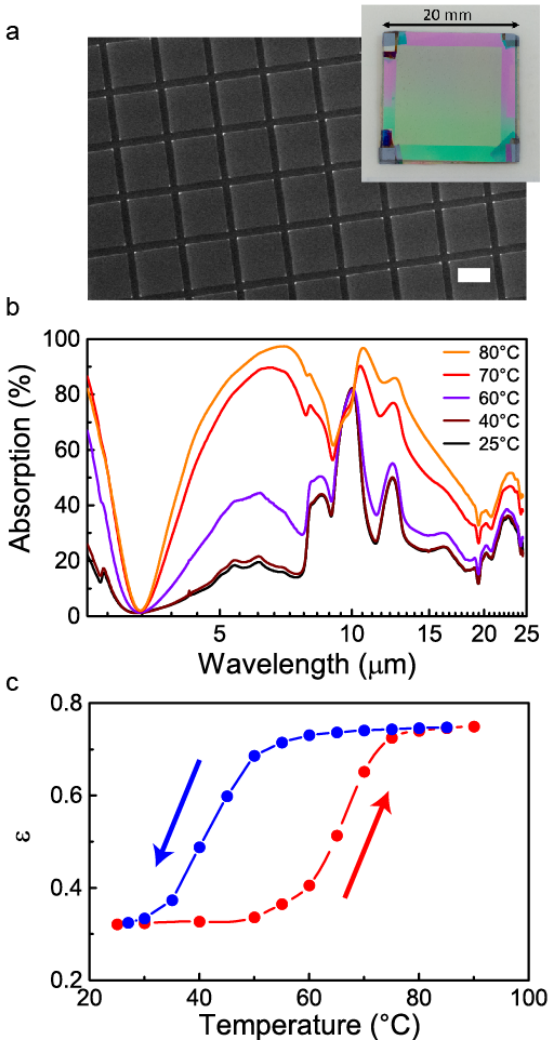

Figure 5 (a) Planar SEM micrograph of the scaled-up VO_2 meta-reflector with a feature size of 2.7 μm and gap of 0.5 μm. Scale bar, 2 μm. The inset shows VO_2 meta-reflectors on 20×20 mm^2 substrate. (b) Absorption spectra of VO_2 meta-reflector of a, measured at 25°C, 40°C, 60°C, 70°C and 80°C (cycle up). (c) Emissivity ε as a function of temperature cycle up and down from 25°C to 90°C as indicated by arrows.

For Table of Contents Only